CHIN. PHYS. LETT. Vol. 36, No. 10 (2019) 107101

Pressure-Induced Metallization Accompanied by Elongated S–S Dimer in Charge Transfer Insulator NiS_2 *

Hao Wu(吴昊)[1,2], Yong-Hui Zhou(周永惠)[2**], Yi-Fang Yuan(袁亦方)[2,3], Chun-Hua Chen(陈春华)[2,3], Ying Zhou(周颖)[2,3], Bo-Wen Zhang(张博文)[2,3], Xu-Liang Chen(陈绪亮)[2], Chuan-Chuan Gu(顾川川)[2], Chao An(安超)[4], Shu-Yang Wang(王舒阳)[2,3], Meng-Yao Qi(戚梦瑶)[4], Ran-Ran Zhang(张冉冉)[2], Li-Li Zhang(张丽丽)[5], Xin-Jian Li(李新建)[1**], Zhao-Rong Yang(杨昭荣)[2,3,4**]

[1]*Department of Physics and Laboratory of Material Physics, Zhengzhou University, Zhengzhou 450052*
[2]*Anhui Province Key Laboratory of Condensed Matter Physics at Extreme Conditions, High Magnetic Field Laboratory, Chinese Academy of Sciences, Hefei 230031*
[3]*University of Science and Technology of China, Hefei 230026*
[4]*Institutes of Physical Science and Information Technology, Anhui University, Hefei 230601*
[5]*Shanghai Synchrotron Radiation Facility, Shanghai Advanced Research Institute, Chinese Academy of Sciences, Shanghai 201204*

(Received 14 June 2019)

The insulator-metal transition triggered by pressure in charge transfer insulator NiS_2 is investigated by combining high-pressure electrical transport, synchrotron x-ray diffraction and Raman spectroscopy measurements up to 40–50 GPa. Upon compression, we show that the metallization firstly appears in the low temperature region at ∼3.2 GPa and then extends to room temperature at ∼8.0 GPa. During the insulator-metal transition, the bond length of S–S dimer extracted from the synchrotron x-ray diffraction increases with pressure, which is supported by the observation of abnormal red-shift of the Raman modes between 3.2 and 7.1 GPa. Considering the decreasing bonding-antibonding splitting due to the expansion of S–S dimer, the charge gap between the S-ppπ^* band and the upper Hubbard band of Ni-3d e_g state is remarkably decreased. These results consistently indicate that the elongated S–S dimer plays a predominant role in the insulator-metal transition under high pressure, even though the p-d hybridization is enhanced simultaneously, in accordance with a scenario of charge-gap-controlled type.

PACS: 71.30.+h, 78.30.Am, 72.20.Dp, 61.05.cp DOI: 10.1088/0256-307X/36/10/107101

Insulator-metal transition (IMT) in electronic strongly correlated systems is an important subject of condensed matter physics and has been studied extensively for several decades.[1,2] As a prototypical electronic strongly correlated material, transition metal disulfide NiS_2 can be driven from insulator to metal by either chemical doping of Se and/or application of external pressure.[2–11] NiS_2 is normally deemed to be a charge transfer insulator in view of the Zaanen–Sawatzky–Allen scheme,[12–15] in which the chalcogen p band is located between upper and lower Hubbard bands of Ni d orbitals. Various measurements have been conducted to explore the charge gap, including transport,[3,16,17] photoemission spectroscopy,[13,18–20] scanning tunneling microscopy,[21] and infrared spectroscopy.[22] Meanwhile, recent work has identified that the main parameter to control the charge gap is the bonding-antibonding splitting in the S–S dimer.[5] Upon substitution of S by Se, the lattice expands due to the larger atomic radius of Se atoms, instead of shrinking as in the case of applying pressure. Therefore, the IMT triggered by Se doping may have a distinct origin from that induced by pressure.

Although the IMT in NiS_2 has been investigated thoroughly, its microscopic mechanism (i.e., bandwidth-controlled type or dominated by a reduction of the charge gap) remains controversial.[22–29] For the case of Se substitution, the IMT was interpreted as the decreased charge gap due to smaller bonding-antibonding splitting,[5,24] as supported by the observed softness of the Se-Se bond.[25] However, low-temperature x-ray diffraction (XRD) and Raman experiments found that, around the IMT, the bond length between Ni and S (Se) ions has a sudden contraction with unnoticeable anomaly in the bond length between chalcogen ions, which demonstrates the dominant role of p-d hybridization in the IMT[26] and is in accordance with the viewpoint of bandwidth-controlled type.[13,27] With the application of pressure, the shrinkage of a lattice normally enhances the band overlapping and further leads to the band broadening. By assuming the rigidity of the S–S dimer, the IMT under pressure is intuitively believed to be controlled by the enhancement of bandwidth of either e_g or p band.[5,22] However, the rigidity of the S–S

*Supported by the National Key Research and Development Program of China under Grant Nos 2018YFA0305700 and 2016YFA0401804, the National Natural Science Foundation of China under Grant Nos 11574323, 11704387, 11874362, 11804344, 11804341, 61774136, 11605276 and U1632275, the Major Program of Development Foundation of Hefei Center for Physical Science and Technology under Grant No 2018ZYFX002, the Users with Excellence Project of Hefei Science Center of Chinese Academy of Sciences under Grant No 2018HSC-UE012, the Natural Science Foundation of Anhui Province under Grant Nos 1808085MA06, 1908085QA18 and 1708085QA19, and the Director's Fund of Hefei Institutes of Physical Science of Chinese Academy of Sciences under Grant No YZJJ201621.
**Corresponding author. Email: yhzhou@hmfl.ac.cn; lixj@zzu.edu.cn; zryang@issp.ac.cn
© 2019 Chinese Physical Society and IOP Publishing Ltd

dimer is not supported by some of the structural investigations, such as high-pressure XRD and Raman experiments,[25,28] in which the potential anomalies of the structure and lattice vibrations were reported. For example, recent single crystal XRD experiments up to 3.86 GPa show a pressure-induced structural transition from cubic to monoclinic at 2.9 GPa and 5 K,[10] whereas no crystal symmetry change at room temperature has been reported so far in polycrystalline up to 10.3 GPa[29] and single crystal up to 5.4 GPa.[28] The inconsistency among different reports could be attributed to the sample quality, on the one hand, because the physical properties of NiS_2 at ambient pressure are found to be strongly sensitive to the real S components.[30] A comprehensive investigation of transport properties and crystal structure under high pressure in the samples with almost the same component is lacking. On the other hand, the pressure range in these investigations is limited (e.g., 3.86 GPa,[10] 5.4 GPa,[28] 11.2 GPa,[25] and 4.2 GPa[11]), which is inadequate to uncover the microscopic mechanism of the IMT, leading to the controversial role of S–S dimers.

In this work, we conduct combined high-pressure electrical transport, synchrotron x-ray diffraction and Raman spectroscopy measurements on the $NiS_{2.02}$ single crystals in diamond anvil cells. By extending the pressure up to 40–50 GPa, these measurements consistently reveal a well-defined IMT zone. It is shown that the IMT, taking place in the pressure region of 3.2–8.0 GPa, is accompanied by the remarkable increase of the bond length between S ions (d_{S-S}). In support of the softness of the S–S dimers, the Raman modes display abnormal red-shift upon compression across the IMT zone. These results confirm that the elongated S–S dimer plays a key role in the metallization, by decreasing the charge gap of pressurized NiS_2.

Single crystals of $NiS_{2.02}$ were grown by a Te-flux method.[31] Room-temperature x-ray diffraction patterns of single crystal and crushed crystal powder were obtained with Cu K_α radiation of wavelength 1.5406 Å using a Rigaku x-ray diffractometer. The atomic proportion of the crystal was characterized via energy dispersive x-ray spectroscopy (EDXS) by combining area- and point-scanning modes. High-pressure resistance measurements were conducted in a screw-pressure-type diamond anvil cell made of BeCu alloy. A pair of anvil culets of 300 μm was used. A piece of single crystal with dimension of $100 \times 30 \times 10\ \mu m^3$ and some ruby powder were loaded into the chamber. Soft NaCl fine powder was the pressure-transmitting medium. The standard four-probe method with a platinum foil electrode was employed, where two probes were used in high-resistance state and four probes in low-resistance state. Pressure was calibrated via the ruby fluorescence scale at room temperature.[32] High-pressure powder x-ray diffraction experiments were carried out at the beamline BL15U1 of Shanghai Synchrotron Radiation Facility (SSRF). A symmetric diamond anvil cell with a culet of 300 μm in diameter was used. Daphne 7373 was served as the pressure-transmitting medium. The wavelength of focused monochromatic x-ray beam was 0.6199 Å for the angle-dispersive diffraction. A Mar345 image plate was used to record 2D diffraction patterns. The DIOPTAS[33] program was used for image integrations and the standard Rietveld refinement was employed by the GSAS.[34] Raman scattering measurements were performed at room temperature on fresh $NiS_{2.02}$ single crystal using a 532 nm solid-state laser for excitation with the power below 1% to avoid sample damage and any heating effect at the China High Magnetic Field Laboratory (CHMFL) in Hefei. A symmetric diamond anvil cell with a culet of 300 μm in diameter was used. Daphne 7373 and NaCl were used as the pressure-transmitting media respectively. Pressure was calibrated via the ruby fluorescence method at room temperature.[32]

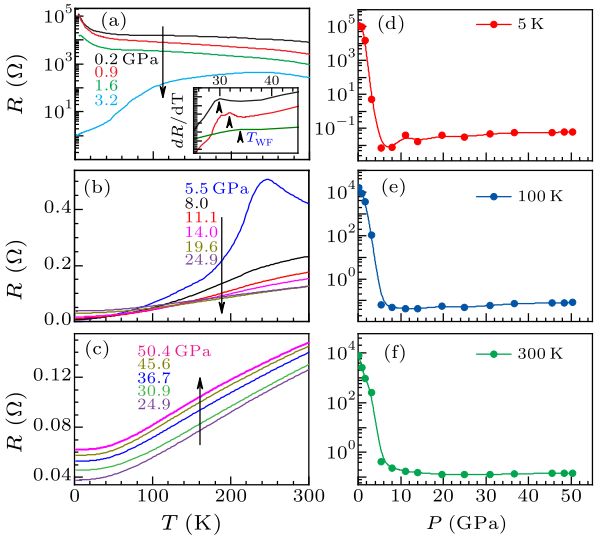


Fig. 1. Temperature-dependent electrical resistance $R(T)$ of $NiS_{2.02}$ single crystal under pressure up to 50.4 GPa. (a) The emergence of pressure-induced metallization within 3.2 GPa. Inset: the derivative of $R(T)$ as a function of temperature. The weak ferromagnetic transition temperature T_{WF} is marked by the arrow. (b), (c) The $R(T)$ curves at representative pressures up to 24.9 GPa and 50.4 GPa, respectively. (d)–(f) The isothermal resistance at 5 K, 100 K and 300 K as a function of pressure.

The synthesized NiS_2 single crystals were characterized by the XRD experiments, which indicate the pure cubic phase of the as-grown crystals with (111) preferential growth orientation. The EDXS characterization yields the near-stoichiometric composition of $NiS_{2.02}$. These results indicate the high quality of the as-grown crystals. To explore how pressure affects the electronic state and hence the transport properties, high-pressure electrical resistance measurements were conducted on the single crystal $NiS_{2.02}$. Figures 1(a)–1(c) show the selected electrical resistance curves $R(T)$ as a function of temperature at various pressures up to 50.4 GPa. At 0.2 GPa, the $R(T)$ curve is similar to that at ambient pressure.[35–39] The weak ferromagnetic temperature T_{WF} that is characterized as a kink in the temperature derivative of the resis-

tance $dR(T)/dT$ increases monotonically upon compression to 1.6 GPa, see the denoted arrows in the inset of Fig. 1(a). The increase of T_{WF} is consistent with previous reports and can be attributed to the enhancement of the exchange interactions under pressure.[10,11] With further increasing pressure, the metallization starts to emerge at 3.2 GPa and completes in the whole temperature region at 8.0 GPa. During the metallization, the resistance is drastically suppressed by 4–6 orders of magnitude, as seen from the isothermal resistance curves at 5 K, 100 K and 300 K in Figs. 1(d)–1(f). Above 8.0 GPa, two regimes with different resistance variations can be identified. Between 8.0 and 24.9 GPa, the high-temperature resistance decreases while the low-temperature resistance increases upon compression. As the pressure is continuously increased from 24.9 GPa to 50.4 GPa, the whole resistance curve globally gets enhanced.

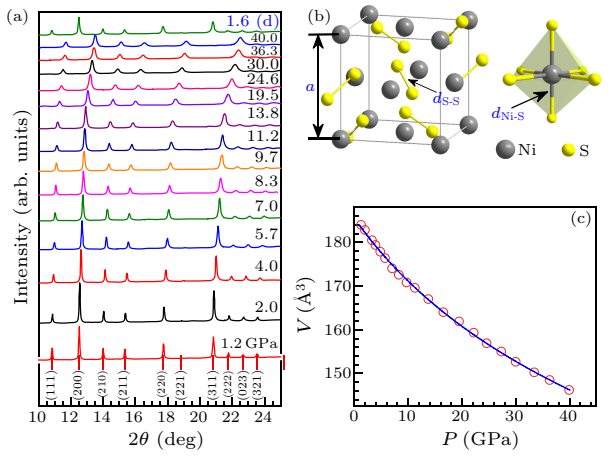


Fig. 2. High-pressure powder synchrotron x-ray diffraction patterns ($\lambda = 0.6199$ Å) and Rietveld refinements of $NiS_{2.02}$ at room temperature. (a) Representative diffraction patterns under compression up to 40.0 GPa and under decompression to 1.6 GPa. For 1.2 GPa, the solid lines and open circles represent the Rietveld refinements for the lattice and observed data, respectively. The vertical bars symbolize the peak positions of $Pa\bar{3}$ phase ($Z = 4$). (b) Schematic crystal structure of pyrite NiS_2 ($Pa\bar{3}$, No. 205) at ambient pressure with NiS_6 octahedron. The two bond lengths d_{Ni-S} and d_{S-S} are indicated by the arrows. The silvery gray and yellow balls represent the Ni and S atoms, respectively. (c) Volume as a function of pressure. The solid lines are the fitting results based on third-order Birch–Murnaghan equation of state.

To study the relationship between IMT and crystal structure in pressurized $NiS_{2.02}$, *in situ* synchrotron XRD measurements were performed on crushed crystal powder up to 40.0 GPa at room temperature. The representative diffraction patterns are presented in Fig. 2(a). At ambient pressure, pyrite NiS_2 has a NaCl-type structure with space group $Pa\bar{3}$ (No. 205), as shown in Fig. 2(b). Upon compression, all peaks move towards high angles and do not show any new peaks throughout the whole pressure range studied, which is similar to the early reports.[28,29] Although a possible structural transition from cubic to monoclinic at low temperature was conjectured,[10] no peak splitting due to symmetry reduction can be detected within our experimental resolution. The XRD patterns up to 40.0 GPa can be well fitted by standard Rietveld refinements with the space group $Pa\bar{3}$. The extracted lattice parameter a decreases gradually with increasing pressure. The absence of structural transition at room temperature is evidenced by the Raman measurements as discussed in the following, and could be further searched for support by comparing with the case of Se doping. For Se doping, no structural transition appears at room temperature since NiS_2 and $NiSe_2$ are isostructural. Figure 2(c) shows the unit cell volume as a function of pressure, which is fitted by the third-order Birch–Murnaghan equation of state.[40] The fitting yields the ambient pressure volume $V = 185.5$ Å^3, bulk modulus $B = 105.8$ GPa, and its first pressure derivative $B' = 3.9$, respectively. Although the volume shrinks monotonically, the extracted bond lengths of Ni–S (d_{Ni-S}) and S–S (d_{S-S}) display anomalies on crossing over the IMT (see text in the following).

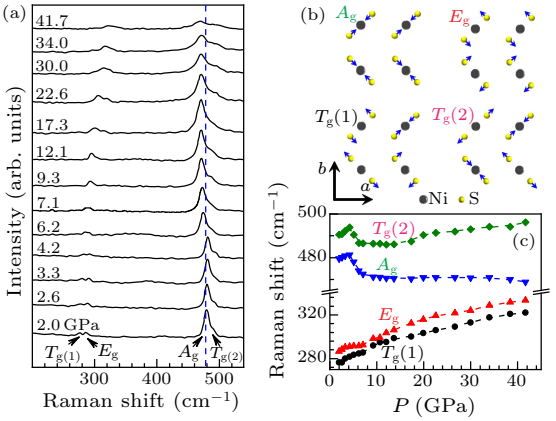


Fig. 3. (a) Representative room temperature Raman spectra of $NiS_{2.02}$ at various pressures up to 41.7 GPa. There are four Raman modes, $T_g(1)$, E_g, A_g and $T_g(2)$, as indicated by the arrows. Blue dashed lines are guide to the eyes. (b) Displacement vectors for the four Raman-active modes of NiS_2 pyrite. (c) Pressure dependence of Raman modes of $NiS_{2.02}$.

Raman spectroscopy is an effective and powerful tool in detecting small lattice distortions, as well as structural transitions. In the NiS_2, since Ni atoms are at the center of inversion, the Raman modes are mainly determined by the displacements of S ions. To carefully check the anomalous evolution of d_{S-S} extracted from the XRD experiments, we further conducted high-pressure Raman spectroscopy measurements at room temperature. Figure 3 shows representative Raman spectra of single crystal $NiS_{2.02}$ at various pressures. According to the space group analysis, five Raman modes are expected for pyrite NiS_2: $A_g + E_g + 3T_g$.[25] At 2.0 GPa, the Raman spectrum exhibits four Raman-active modes, in agreement with the ambient results.[25] As shown in Fig. 3(b), the low-frequency $T_g(1)$ and E_g modes correspond to the S–S pair liberations, and the high-frequency A_g and $T_g(2)$ modes symbol the in-phase and out-of-phase stretching vibrations of the S–S pairs.[25,41–43] No additional

Raman modes are observed up to 41.7 GPa. With increasing pressure, although Raman modes $T_g(1)$ and E_g display blue-shift due to the lattice compression, the other two modes A_g and $T_g(2)$ exhibit distinctly abnormal red-shift between 3.2 GPa and 7.1 GPa, see Fig. 3(c). This abnormal red-shift behavior directly reflects the softness of the S–S dimer, which is in line with the XRD results. We note that the high-pressure Raman spectra investigated by Marini *et al.* also revealed anomaly near the IMT.[25] Nevertheless, they reported the splitting of S–S stretching mode A_g around 3.8 GPa, which is clearly in disagreement with our case. This discrepancy could be caused by the difference in either sample quality or pressure-transmitting medium. Marini *et al.* have performed measurements on polycrystalline sample using NaCl as the transmitting medium, in contrast to single crystal and Daphne 7373 in our case. To make a more detailed study of the abnormal red-shift of the Raman modes, we have made another elaborate measurement by increasing pressure with smaller steps. In addition, in view of the different pressure-transmitting medium which may lead to the peaking splitting, we have added a reference experiment with NaCl as the pressure-transmitting medium. We note that the spectra do not show any peak splitting of A_g mode up to around 11 GPa for both NaCl and Daphne 7373. Moreover, the evolution of spectra under pressure is almost reproducible for different runs. Both A_g and $T_g(2)$ modes display a distinct red-shift irrelative to the pressure medium (see text in the following).

Once we combine the above electrical transport, XRD and Raman data, a close relationship between the resistance and the elongated S–S dimer under pressure is clearly displayed, as outlined in Fig. 4. Upon compression, as seen from Fig. 4(a), the metallization firstly takes place at low temperatures around P_{c1} and then finishes in the whole temperature region at P_{c2}, forming a well-defined IMT zone. The proceeding of IMT from P_{c1} to P_{c2} is completely accompanied by the abnormal elongation in the d_{S-S} and softness of the S–S dimer, demonstrating strong electron-lattice coupling in the IMT, as shown in Figs. 4(b) and 4(c). NiS_2 is a charge transfer insulator, with the band structure described by three fundamental parameters: bandwidth, Coulomb repulsion, and charge gap. The bandwidth is determined by the hybridization of Ni and S ions while the charge gap is associated with S–S dimer. With the expansion of S–S dimer, the bonding-antibonding splitting becomes smaller and so does the charge gap. Accordingly, the IMT driven by pressure is in accordance with the scenario of charge-gap-controlled type. Nevertheless, it should be pointed out that the contribution from p–d hybridization cannot be excluded completely because d_{Ni-S} also decreases more steeply in this region. Outside the IMT zone, both d_{S-S} and Raman modes display a normal pressure dependence.

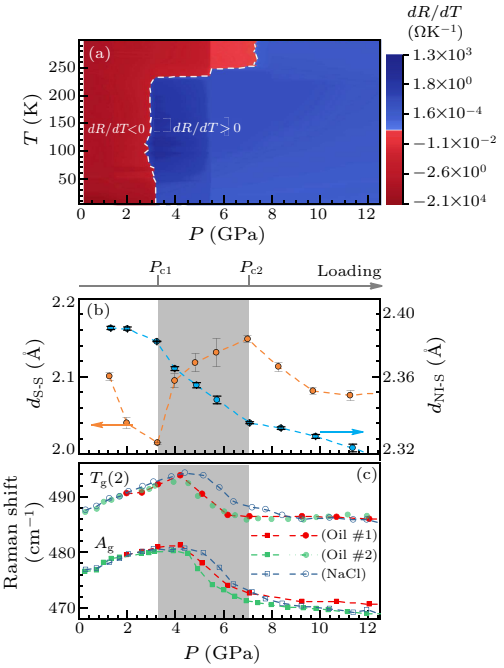


Fig. 4. The first derivative of resistance of single-crystal $NiS_{2.02}$ under P–T conditions and its relations to the bond length d_{Ni-S}, d_{S-S} and two Raman modes A_g and $T_g(2)$ in three runs. The white dashed line in (a) displays the boundary between insulating and metallic states. With increasing pressure, there is a transition between $P_{c1}\sim$3.2 GPa and $P_{c2}\sim$ 7.1 GPa, as indicated by the gray shadow areas in (b) and (c).

In summary, we have studied the high pressure electronic and structural properties of single crystal $NiS_{2.02}$. All the measurements, including electrical transport, XRD and Raman spectroscopy, consistently reveal two critical pressure points P_{c1} and P_{c2}. On going from P_{c1} to P_{c2}, the metallization first appears at low temperatures, then extends gradually to the whole temperature region. Meanwhile, the S–S dimer displays a softness behavior, as reflected by the elongation of d_{S-S} and red-shift of Raman modes. As the S–S dimer is elongated, the charge gap decreases and closes finally at the critical pressure. This finding highlights the role of S–S dimer in triggering the IMT under pressure, and sheds light on the understanding of the origin of IMT in other electronic strongly correlated systems.

References

[1] Mott N F 1968 *Rev. Mod. Phys.* **40** 677
[2] Imada M, Fujimori A and Tokura Y 1998 *Rev. Mod. Phys.* **70** 1039
[3] Yao X, Honig J M, Hogan T, Kannewurf C and Spałek J 1996 *Phys. Rev. B* **54** 17469
[4] Bouchard R J, Gillson J L and Jarrett H S 1973 *Mater. Res. Bull.* **8** 489
[5] Kuneš J, Baldassarre L, Schächner B, Rabia K, Kuntscher C A, Korotin D M, Anisimov V I, McLeod J A, Kurmaev E Z and Moewes A 2010 *Phys. Rev. B* **81** 035122
[6] Mori N, Mitsui T and Yomo S 1973 *Solid State Commun.* **13** 1083
[7] Husmann A, Jin D S, Zastavker Y V, Rosenbaum T F, Yao X and Honig J M 1996 *Science* **274** 1874

[8] Miyasaka S, Takagi H, Sekine Y, Takahashi H, Môri N and Cava R J 2000 *J. Phys. Soc. Jpn.* **69** 3166
[9] Niklowitz P G, Alireza P L, Steiner M J, Lonzarich G G, Braithwaite D, Knebel G, Flouquet J and Wilson J A 2008 *Phys. Rev. B* **77** 115135
[10] Feng Y, Jaramillo R, Banerjee A, Honig J M and Rosenbaum T F 2011 *Phys. Rev. B* **83** 035106
[11] Friedemann S, Chang H, Gamża M B, Reiss P, Chen X, Alireza P, Coniglio W A, Graf D, Tozer S and Grosche F M 2016 *Sci. Rep.* **6** 25335
[12] Zaanen J, Sawatzky G A and Allen J W 1985 *Phys. Rev. Lett.* **55** 418
[13] Matsuura A Y, Shen Z X, Dessau D S, Park C H, Thio T, Bennett J W and Jepsen O 1996 *Phys. Rev. B* **53** R7584
[14] Bocquet A E, Mizokawa T, Saitoh T, Namatame H and Fujimori A 1992 *Phys. Rev. B* **46** 3771
[15] Honig J M and Spałek J 1998 *Chem. Mater.* **10** 2910
[16] Kwizera P, Dresselhaus M S and Adler D 1980 *Phys. Rev. B* **21** 2328
[17] Matsuura M, Hiraka H, Yamada K and Endoh Y 2000 *J. Phys. Soc. Jpn.* **69** 1503
[18] Matsuura A Y, Watanabe H, Kim C, Doniach S, Shen Z X, Thio T and Bennett J W 1998 *Phys. Rev. B* **58** 3690
[19] Mamiya K, Mizokawa T, Fujimori A, Miyadai T, Chandrasekharan N, Krishnakumar S R, Sarma D D, Takahashi H, Môri N and Suga S 1998 *Phys. Rev. B* **58** 9611
[20] Krishnakumar S R and Sarma D D 2003 *Phys. Rev. B* **68** 155110
[21] Iwaya K, Kohsaka Y, Satow S, Hanaguri T, Miyasaka S and Takagi H 2004 *Phys. Rev. B* **70** 161103
[22] Perucchi A, Marini C, Valentini M, Postorino P, Sopracase R, Dore P, Hansmann P, Jepsen O, Sangiovanni G, Toschi A, Held K, Topwal D, Sarma D D and Lupi S 2009 *Phys. Rev. B* **80** 073101
[23] Xu H C, Zhang Y, Xu M, Peng R, Shen X P, Strocov V N, Shi M, Kobayashi M, Schmitt T, Xie B P and Feng D L 2014 *Phys. Rev. Lett.* **112** 087603
[24] Schuster C, Gatti M and Rubio A 2012 *Eur. Phys. J. B* **85** 325
[25] Marini C, Perucchi A, Chermisi D, Dore P, Valentini M, Topwal D, Sarma D D, Lupi S and Postorino P 2011 *Phys. Rev. B* **84** 235134
[26] Han G, Choi S, Cho H, Sohn B, Park J G and Kim C 2018 *Phys. Rev. B* **98** 125114
[27] Moon C Y, Kang H, Jang B G and Shim J H 2015 *Phys. Rev. B* **92** 235130
[28] Fujii T, Tanaka K, Marumo F and Noda Y 1987 *JOM* **13** 448
[29] Endo S, Mitsui T and Miyadai T 1973 *Phys. Lett. A* **46** 29
[30] Krill G, Lapierre M F, Robert C, Gautier F, Czjzek G, Fink J and Schmidt H 1976 *J. Phys. C* **9** 761
[31] Yao X and Honig J M 1994 *Mater. Res. Bull.* **29** 709
[32] Mao H K, Xu J and Bell P M 1986 *J. Geophys. Res.* **91** 4673
[33] Prescher C and Prakapenka V B 2015 *High Press. Res.* **35** 223
[34] Toby B H 2001 *J. Appl. Crystallogr.* **34** 210
[35] Matsuura M, Endoh Y, Hiraka H, Yamada K, Mishchenko A S, Nagaosa N and Solovyev I V 2003 *Phys. Rev. B* **68** 094409
[36] Higo T and Nakatsuji S 2015 *J. Phys. Soc. Jpn.* **84** 053702
[37] Thio T and Bennett J W 1994 *Phys. Rev. B* **50** 10574
[38] Sarma D D, Krishnakumar S R, Weschke E, Schüßler-Langeheine C, Mazumdar C, Kilian L, Kaindl G, Mamiya K, Fujimori S I, Fujimori A and Miyadai T 2003 *Phys. Rev. B* **67** 155112
[39] Clark C and Friedemann S 2016 *J. Magn. Magn. Mater.* **400** 56
[40] Birch F 1947 *Phys. Rev.* **71** 809
[41] Suzuki T, Uchinokura K, Sekine T and Matsuura E 1977 *Solid State Commun.* **23** 847
[42] Lemos V, Gualberto G M, Salzberg J B and Cerdeira F 1980 *Phys. Status Solidi B* **100** 755
[43] Kleppe A K and Jephcoat A P 2004 *Mineral. Mag.* **68** 433